The length scale measurements of the fractional quantum Hall state on a cylinder

2015 New J. Phys. 17 095006

(http://iopscience.iop.org/1367-2630/17/9/095006)

New Journal of Physics
The open access journal at the forefront of physics

Deutsche Physikalische Gesellschaft DPG
IOP Institute of Physics

Published in partnership with: Deutsche Physikalische Gesellschaft and the Institute of Physics

OPEN ACCESS

RECEIVED
27 May 2015

REVISED
5 August 2015

ACCEPTED FOR PUBLICATION
2 September 2015

PUBLISHED
24 September 2015

PAPER

The length scale measurements of the fractional quantum Hall state on a cylinder

Qi Li, Na Jiang, Zheng Zhu and Zi-Xiang Hu

Department of Physics, Chongqing University, Chongqing, 401331, People's Republic of China

E-mail: zxhu@cqu.edu.cn

Keywords: Laughlin state, tunneling, entropy

Abstract

Once the fractional quantum Hall (FQH) state for a finite-sized system is put on the surface of a cylinder, the distance between the two ends with open boundary conditions can be tuned by varying the aspect ratio γ. It scales linearly with increasing the system size and therefore has a larger adjustable range than that on a disk. The previous study of the quasi-hole tunneling amplitude on a disk by Hu *et al* (2011 *New J. Phys.* **13** 035020) indicates that the tunneling amplitudes have a scaling behavior as a function of the tunneling distance and the scaling exponents are related to the scaling dimension and the charge of the transported quasiparticles. However, the scaling behaves poorly due to the narrow range of the tunneling distance on the disk. Here we systematically study the quasiparticle tunneling amplitudes of the Laughlin state in the cylinder geometry which shows a much better scaling behavior. In particular, there are some crossover behaviors at the two length scales when the two open edges are close to each other. These lengths are also reflected in the bipartite entanglement and the electron Green's function as either a singularity or a crossover. These two critical length scales of the edge–edge distance, $L_x^{c_1}$ and $L_x^{c_2}$, are found to be related to the dimension reduction and back scattering point respectively.

1. Introduction

The strongly correlated electron system reveals plenty of non-trivial properties beyond the single-particle picture. The fractional quantum Hall effect (FQHE) [1] is a paradigm of strongly correlated system that occurs in a two-dimensional electron gas with a perpendicular magnetic field. The FQH state is one of the most studied objects in condensed matter physics and has a topological protected ground state and non-trivial excitation. In particular, the FQH states on the second Landau level, such as $\nu = 5/2$ and $\nu = 12/5$, are expected to have non-Abelian excitations and have potential applications in topological quantum computation [2–4]. Quasiparticle tunneling through narrow constrictions or point contacts that bring counter-propagating edges close could serve as a powerful tool for probing both the bulk topological order and the edge properties of fractional quantum Hall liquids. In particular, interference signatures from double point contact devices may reveal the statistical properties of the quasiparticles that tunnel through them [5], especially the non-Abelian ones [6, 7]. In disk geometry, a quasiparticle can tunnel from the center to the edge by a single particle tunneling potential $V_{\text{tunnel}} = V_t \delta(\theta)$ which breaks the rotational symmetry [8]. The ring shape of the Landau basis wave function with angular momentum $m\hbar$ on the disk, i.e. $\varphi_m(r) \sim \mathbf{r}^m \mathrm{e}^{-|r|^2/4}$, has radius $\sqrt{2m}\, l_B$. Therefore the tunneling distance d is tuned by inserting N_{qh} flux quantum, or N_{qh} quasiholes at the center, namely $d/l_B = \sqrt{2(N_{\text{orb}} + N_{qh})} - \sqrt{2N_{qh}}$ where N_{orb} is the number of orbitals. The shape of the system evolves from disk to annulus and finally to a quasi-1D ring with increasing N_{qh}. In the ring limit (or CFT limit) with $d \to 0$, or $N_{qh} \to \infty$, we found a universal analytical formula for the tunneling amplitudes of the bulk quasihole [9] and the edge excitations [10]. On the other hand, the quasihole tunneling amplitudes were found to have a scaling behavior as a function of the system size N_e and the tunneling distance d. Interestingly, the fractional charge and the scaling dimension appear in the exponents of the scaling function [9]. However, if we look carefully at the

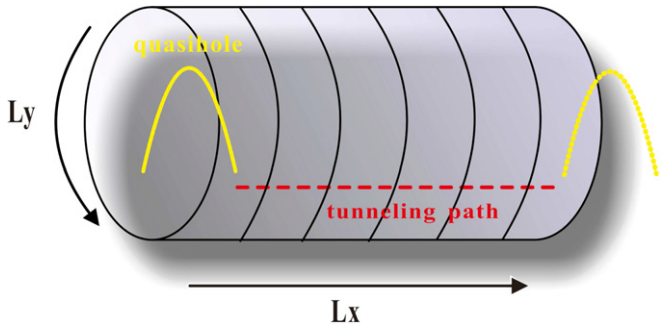

Figure 1. The sketch of the quasiparticle tunneling from one side to the other side of the cylinder. The tunneling path is given by a potential $V_{\text{tunnel}} = V_t \delta(y)$ which has length L_x.

data of the tunneling amplitude in disk geometry, the scaling function does not work very well for small d which was treated as a finite size effect [8] due to the fact that a limited number of electrons can be handled in the numerical diagonalization. It is also hard to look into this region on a disk since $N_{qh} \to \infty$ while $d \to 0$.

In this paper, we alternatively consider the physics properties of the FQH liquid in the cylinder geometry. The cylinder has as its advantages the fact that the distance between the two ends is proportional to the system size and can be tuned from zero to infinity smoothly by varying the aspect ratio $\gamma = L_y/L_x$, where L_y is the circumference on the side with periodic boundary and L_x is the length of the finite cylinder with open boundaries. As a comparison, in the disk geometry, the tunneling distance has a maximum which is the radius of the system $R = \sqrt{2N_{\text{orb}}}$ and $d \sim N_{\text{orb}}/\sqrt{2N_{qh}}$ for $N_{qh} \gg N_{\text{orb}}$. This is very inconvenient when we want to look at the small d region since numerous quasiholes or flux will be inserted at the center of the disk. On the other side, when $\gamma \to 0$, namely in the thin cylinder limit, the two adjacent Landau orbitals have practically zero overlap. In this case, the Hamiltonian is dominated by the electrostatic repulsion which contains the direct interaction $\langle \varphi_m \varphi_n | V | \varphi_n \varphi_m \rangle$ and the exchange interaction $\langle \varphi_m \varphi_n | V | \varphi_m \varphi_n \rangle$. The ground state is generally called a charge density wave (CDW) state, or Tao–Thouless (TT) crystal state [11, 12] on the torus with the electronic occupation pattern $1001001001\cdots$ in order to minimize the electrostatic repulsion energy. The wave function of the FQH state [13] can be obtained by diagonalizing the model Hamiltonian with hardcore interaction, or the Hamiltonian only with $V_1 \neq 0$ in the language of Haldane's pseudopotential. The more interesting case is when $\gamma \to \infty$ or $L_y \to \infty$, to keep the total area of the surface $L_x L_y = 2\pi l_B^2 N_{\text{orb}}$ invariant; to keep the total penetrated flux invariant, L_x then approaches zero. It means the two-counter-propagating edges at the two ends of the cylinder are coming close to each other and the system finally evolves into a one-dimensional system. In this case, because of the strong overlap of all the Landau orbitals, the Gaussian factors of each Landau wavefunction are the same and can be erased by normalization. In this one-dimensional limit, the FQH wave function can be described by the Jack polynomials and therefore all the results are the same as those that we did on the disk in the ring limit. The Jack polynomial is one of the polynomial solutions for the Calogero–Sutherland Hamiltonian [14] which can describe the Read–Rezayi Z_k-parafermion states with a negative parameter α and a root configuration (or partition). The Jack polynomial is a powerful method in studying the FQHE as it can construct not only the model wave function for the Read–Rezayi series [15–17], but also the low-lying excitations [18, 19]. Another advantage of the cylinder geometry is its computational convenience compared with either the disk or sphere geometries which were discussed in the density matrix renormalization calculation [20]. In this paper, we reconsider the quasiparticle tunneling with cylinder geometry especially in the region of small tunneling distance. Here the quasiparticle can tunnel from one edge to the other as sketched in figure 1. Thus the tunneling distance equals the length L_x of the system. We find a richer structure in this region and two characteristic length scales appear not only in the quasiparticle tunneling, but also in the wavefunction overlap, bipartite entanglement entropy and electron Green's function.

The rest of this paper is organized as follows. In section 2, we consider the tunneling amplitude while varying the length of the finite cylinder for $e/3$ and $2e/3$ quasiholes in the Laughlin state. In section 3, the bipartite entanglement entropy, both in orbital space and real space is discussed. The results of the electron Green's functions are discussed in section 4 and summaries and discussions are in section 5.

2. Quasiparticle tunneling for Laughlin state

For electrons on a cylinder with circumference L_y in the y-direction in a magnetic field perpendicular to the surface, the single electron wave function in the lowest Landau level is:

$$\psi_j\left(\vec{r}\right) \equiv |j\rangle = \frac{1}{\sqrt{\pi^{1/2}L_y}} e^{ik_y y} e^{-\frac{1}{2}\left(x+k_y\right)^2} \tag{1}$$

in which $k_y = \frac{2\pi}{L_y} j$, $j = 0, \pm 1, \pm 2\cdots$ are the transitional momentum along the y-direction. Here the magnetic length $l_B = \sqrt{\hbar c/eB}$ has been set as the unit. For a finite-sized system, the number of basis states or orbits, $N_{\rm orb}$, equals the amount of magnetic flux quantum penetrating from the surface. Each orbit occupies an area $2\pi l_B^2$. Therefore, the length in the x-direction for a finite system is fixed with a given aspect ratio γ, namely $L_x/l_B = \sqrt{N_{\rm orb} 2\pi/\gamma}$.

To study the quasiparticle tunneling of the Laughlin state at $\nu = 1/3$, a quasihole with charge $e/3$ or $2e/3$ is put on one edge of the cylinder as shown in figure 1. Here the model wavefunction for the Laughlin state can be obtained by diagonalizing the model Hamiltonian with hardcore interaction, or just $V_1 \neq 0$ in the language of the Haldane's pseudopotential. It can also be obtained by using the Jacks with the so-called root configuration $1001001001\cdots$. The quasihole state for $e/3$ and $2e/3$ is just the translated state with one and two sites along the x-direction respectively. Alternately, we can say a quasihole is inserted at the left edge of the finite cylinder which is represented as roots $01001001001\cdots$ and $001001001001\cdots$ for $e/3$ and $2e/3$ respectively in the Jack polynomial description. A simple single-particle tunneling potential

$$V_{\rm tunnel} = V_t \delta(y)$$

is assumed. It describes a tunneling path along the x-direction and therefore breaks the translational symmetry in the y-direction. Then the matrix element is $\langle k|V_{\rm tunnel}|m\rangle$, which is related to the tunneling of an electron from the single particle state $|m\rangle$ to state $|k\rangle$, is (set $V_t = 1$)

$$v_p(k, m) = \left\langle k \middle| V_{\rm tunnel} \middle| m \right\rangle = e^{-\frac{\pi^2}{L_y^2}(m-k)^2}. \tag{2}$$

It is clear that $v_p(k, m) = e^{-\left(\frac{2\pi}{L_y}m - \frac{2\pi}{L_y}k\right)^2/4} = e^{-(d/l_B)^2/4}$ where d is the distance between the two Gaussians. The many-body tunneling operator can be written as the summation of those for the single particle $\tau = V_t \sum_i \delta(y_i)$. Then we can calculate the tunneling amplitude for many-body wave function $\Gamma = \langle \Psi_{qh}|\tau|\Psi_0\rangle$ in which $|\Psi_0\rangle$ and $|\Psi_{qh}\rangle$ are the ground state and quasihole state wave function respectively. In this section, we just consider the tunneling amplitudes for the $e/3$ and $2e/3$ quasiholes in Laughlin state at $\nu = 1/3$. The matrix elements consist of contributions from the respective Slater-determinant components $|m_1, \ldots, m_N\rangle \in \Psi_0$ and $|k_1, \ldots, k_N\rangle \in \Psi_{qh}$. There are nonzero contributions only when the two sets $m_1, \ldots, m_N$ and $k_1, \ldots, k_N$ are identical except for a single pair m' and k' with angular momentum difference $k' - m' = N$ for $e/3$ and $k' - m' = 2N$ for $2e/3$ where N is the number of electrons. Therefore, we have $v_p^{e/3} = e^{-\frac{\pi^2}{L_y^2}N^2}$ and $v_p^{2e/3} = e^{-\frac{\pi^2}{L_y^2}(2N)^2}$. The tunneling amplitude in the second quantization can be written as:

$$\Gamma = \left\langle \Psi_{qh} \middle| \tau \middle| \Psi_0 \right\rangle = \sum_i \left\langle k_1 k_2 \cdots k_n \middle| \delta\left(y_i\right) C_k^+ C_m \middle| m_1 m_2 \cdots m_n \right\rangle.$$

From equation (2), it is known that the tunneling amplitude decreases exponentially with increasing the tunneling distance which is proportional to $|m - k|$. The distance of the quasiparticle tunneling of the many-body state, or the length of the cylinder L_x, is determined by the size of the system and the aspect ratio γ. For an N-particle system at fixed filling factor, L_x can be tuned from 0 to ∞ by changing the aspect ratio γ. As with the disk, numerous quasiholes were added at the center which makes the radius change from $\sqrt{2N_{\rm orb}}$ to 0. With a given L_y, the distance between two single-particle orbitals on the cylinder is a constant which makes the tunneling distance scale proportional to the system size, i.e. $d \propto N$ on the cylinder compared with $d \propto N^{1/2}$ on the disk. The linear relation guarantees a smooth change while varying γ.

Figures 2(a) and (b) show the tunneling amplitudes for the $e/3$ and $2e/3$ Laughlin quasiholes as a function of the tunneling distance L_x. When $L_x \to \infty$, or $\gamma \to 0$, the system is in a thin cylinder limit and the ground state is a crystal-like state in which electrons are separated; then the quasiparticle cannot tunnel from one side to another, i.e. $\Gamma \to 0$. On the other side, when $L_x \to 0$, or $\gamma \to \infty$, all the single particle orbitals collapse onto each other which corresponds to the ring limit on disk, or the CFT limit in which case the geometry factor of the many-body wave function can be neglected. Our previous studies [9, 10] show that the tunneling amplitude for $e/3$ and $2e/3$ quasiholes in the CFT limit for a system with N electrons can be exactly represented as:

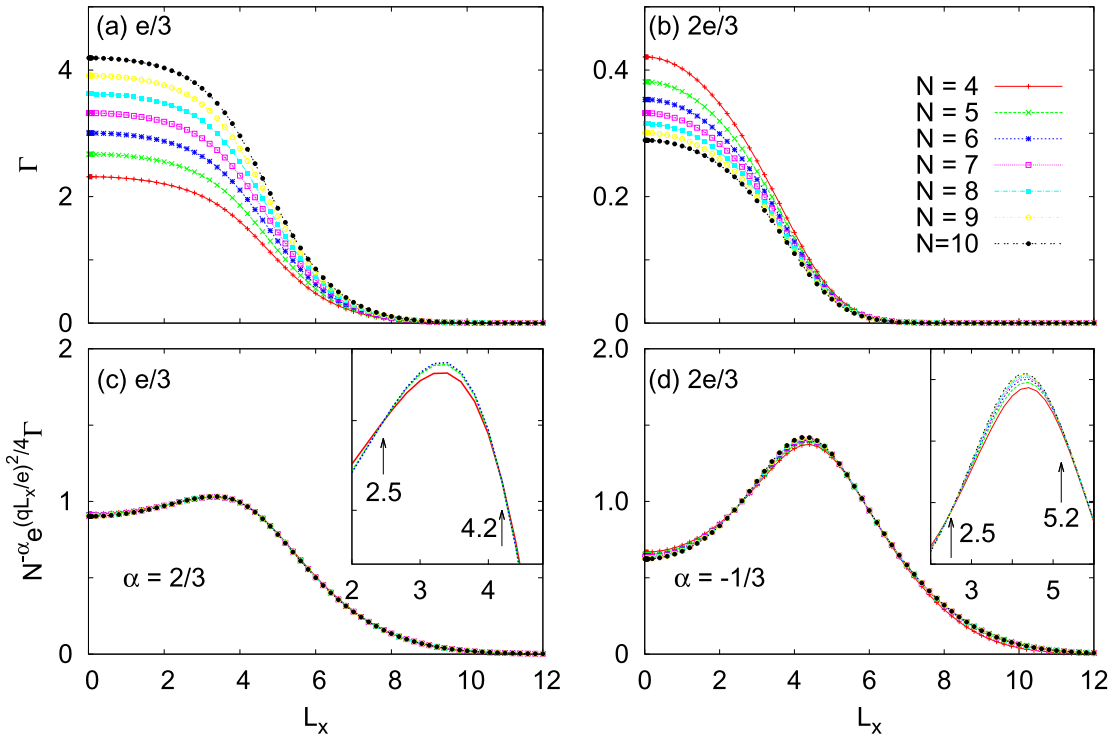

Figure 2. The tunneling amplitude Γ as a function of tunneling distance L_x for $e/3$ (a) and $2e/3$ (b) Laughlin quasihole for system with 4−10 electrons. The data from different systems collapse into a single curve with a scaling function in equation (4). The exponents are $\alpha^{e/3} = 2/3$ (c) and $\alpha^{e/3} = -1/3$ (d) for the two types of quasiholes. The inset figure shows the enlarged rescaled data for small L_x. Some crossover points are labeled by arrows.

$$\Gamma^{e/3}(N) = N\frac{\Omega(1001001\ldots01001)}{\Omega(01001001\ldots01001)}$$
$$\Gamma^{2e/3}(N) = 2!N\frac{\Omega\begin{pmatrix}001001001\ldots001\\1001001001\ldots001\end{pmatrix}}{\Omega\begin{pmatrix}01001001001\ldots001\\001001001001\ldots001\end{pmatrix}} \tag{3}$$

where $\Omega(1001001\ldots01001) = 1\times 3\times 6\times\ldots$ and $\Omega\binom{\mu}{\lambda} = \Omega(\mu)\Omega(\lambda)$. For example, $\Gamma^{e/3}(2) = 2^{\frac{1\times 3}{1\times 4}} = 1.5$ and $\Gamma^{2e/3}(2) = 2\times 2^{\frac{2\times 3}{1\times 2\times 4\times 5}} = 0.6$. The numbers in the fractions are the position of the 1 s in equation (3). Formally, the tunneling amplitude for $e/3$ quasihole for Laughlin state has an algebraic expression $\Gamma^{e/3}(N) = \frac{N}{M}B(N, \frac{1}{M})$, in which $M = 1/\nu = 3$ for the Laughlin state and the beta function B is defined as $B(x, \beta) = \Gamma(x)\Gamma(\beta)/\Gamma(x+\beta)$. Figures 2(a) and (b) show that the tunneling amplitudes saturates exactly at these CFT limit values when $L_x \to 0$. In the medium region of L_x, the tunneling amplitude has a dramatic change from these CFT values to zero. The state in this region is close to the Laughlin state, thus the signal of the decreasing of the quasihole tunneling amplitude can be seen as a measurement of a phase transition (PT)-like from the thin cylinder state with zero tunneling amplitude to the CFT limit with a finite tunneling amplitude. Here we should note that we use the terminology PT-like instead of PT since there is actually no phase transition in the ground state while varying L_x. The topological properties of the ground state in the CFT limit are the same as those in the thin cylinder limit [21–23]. As shown in figures 2(c) and (d), the data for different system sizes collapse into each other after the following scaling conjecture is applied

$$\Gamma^q\left(N, L_x\right) = \Gamma_0 N^{-\alpha^q} e^{\left(qL_x/2el_B\right)^2}. \tag{4}$$

The exponent α^q is related to the scaling dimension of the quasiparticle as $\alpha^q = 1 - 2\Delta^q$. The $\nu = 1/3$ Laughlin quasihole operator can be written as $\psi_{qh} = e^{i\phi m/\sqrt{3}}$ with a primary charge bosonic field ϕ in CFT. Therefore, the scaling dimension for the $e/3$ and $2e/3$ quasiholes are $\Delta^{e/3} = 1/6$ and $\Delta^{2e/3} = 2/3$ respectively and then $\alpha^{e/3} = 2/3$ and $\alpha^{2e/3} = -1/3$. In disk geometry [8], the best scaling parameter for $2e/3$ was $\alpha^{2e/3} = -0.4$ which has a large deviation from the theoretical prediction. We think this deviation should come from the insufficient tunneling distance which is maximized at the radius of the disk. On the other hand, as we

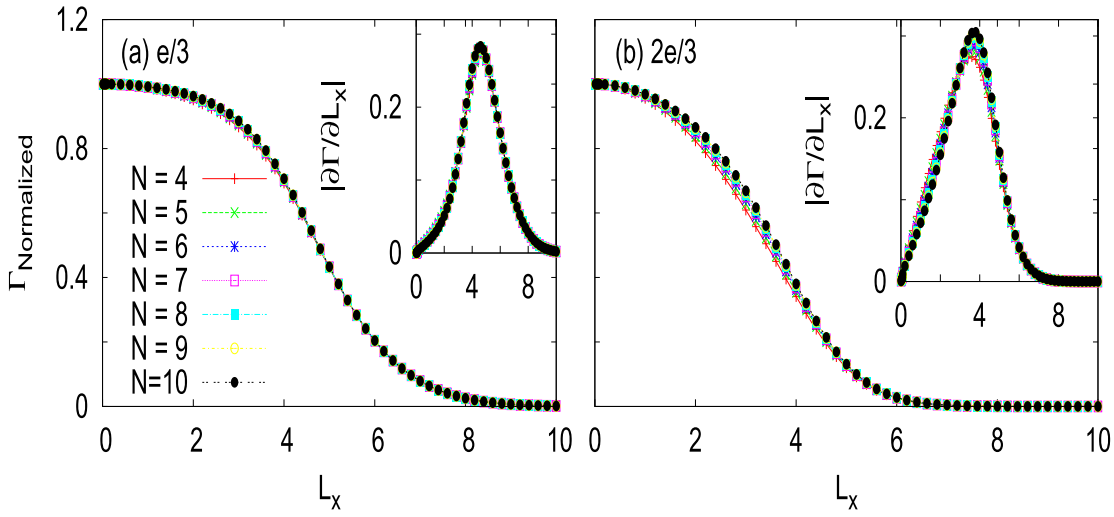

Figure 3. (a) The normalized tunneling amplitude as a function of tunneling distance for the $e/3$ (a) and $2e/3$ quasihole (b). The inset figures are their first-order derivations which have peaks at $L_x^{c_2} \simeq 4.2l_B$ both for $e/3$ (a) and $2e/3$ (b) by extrapolating to $N \to \infty$.

discussed above, the tunnel amplitude data near $d = 0$ is missed due to the huge number of quasiholes needed to be inserted at the center. On the cylinder, as shown in figures 2(c) and (d), the scaling conjecture of equation (4) works perfectly when L_x is larger than a specific value. The reason we are saying this is that if we enlarge the rescaled data in the small L_x region as shown in the inset figure, crossover behaviors from different systems occur around $L_x^{c_1} \simeq 2.5l_B$ and $L_x^{c_2} \simeq 4.2l_B$ as shown by the arrows in figure 2(c). The crossover at $L_x^{c_1} \simeq 2.5l_B$ also remained the same in figure 2(d) for the $2e/3$ quasihole. Here we should note that there is no crossover for larger L_x in figure 2(d). However, we observe that the scaling behavior starts to break down near $L_x^{c_2'} \simeq 5.2l_B$. The first crossover at $L_x^{c_1} \simeq 2.5l_B$ can be explained as a transition from a two-dimensional system to a one-dimensional system. The 1D system corresponds to the Calogero–Sutherland model [24] which actually is the origin of the holomorphic part of the FQH wave function, or the Jack polynomials [15–17]. The dimension reduction of the FQH state was also considered in the composite fermion systems [25, 26]. Alternately, we can say that the system is in the CFT limit while $L_x < L_x^{c_1}$. The second critical value $L_x^{c_2} \simeq 4.2l_B$ for $e/3$ and $L_x^{c_2'} \simeq 5.2l_B$ for $2e/3$ is the transition point where the scaling behavior is broken down. This can be explained by the breaking down of tunneling behavior between the two independent edges due to gluing the two anti-propagating edges together when varying γ. Alternately, we can say that $L_x^{c_2}$ is the length scale at which the two edges start to interact with each other. When $L_x < L_x^{c_2}$, there are back scatterings between the two anti-propagating edges. The different values of $L_x^{c_2}$ between the $e/3$ and $2e/3$ quasiholes should be from their size difference. Another way to extrapolate the critial point $L_x^{c_2}$ is by renormalizing the data by its CFT value from equation (3) as shown in figure 3. Interestingly, the data for different sizes have a scaling-like behavior that collapses into one curve. The inset plots in figure 3 are the first-order deviations of the normalized tunneling amplitudes. Again the first deviations have peaks at $L_x^{c_2} \simeq 4.2l_B$ both for $e/3$ and $2e/3$ by extrapolating to the thermodynamic limit with $N \to \infty$.

On the other hand, besides the N-dependence of the tunneling amplitudes, equation (4) tells us that the ratio of the two types of tunneling amplitude is expected to have an asymptotic behavior which depends on L_x:

$$\frac{\Gamma^{2e/3}}{\Gamma^{e/3}} \sim \mathrm{e}^{-\left[\left(2L_x/3\right)^2-\left(L_x/3\right)^2\right]/\left(2l_B\right)^2} \approx \mathrm{e}^{-0.083\left(L_x/l_B\right)^2}. \tag{5}$$

In figure 4, we plot the ratio $\Gamma^{2e/3}/\Gamma^{e/3}$ as a function of L_x for a system with 6−10 electrons. Unlike the data on a disk [8] in which there was a sudden change while the first quasihole was inserted at the center, the ratio on the cylinder is smooth as a function of L_x. The data in figure 4 can be fitted by a solid line with $\Gamma^{2e/3}/\Gamma^{e/3} \approx \mathrm{e}^{-0.078(x/l_B)^2}$ which is consistent with the expected behavior in equation (5). Compared to the disk, the ratio of the tunneling amplitude for $e/4$ and $e/2$ for the Moore–Read state on the disk has an asymptotic $\Gamma^{e/2}/\Gamma^{e/4} \approx \mathrm{e}^{-0.083(d/l_B)^2}$ which has a relatively large deviation from the expected behavior $\Gamma^{e/2}/\Gamma^{e/4} \approx \mathrm{e}^{-0.047(d/l_B)^2}$. For the Laughlin state, the numerical and theoretical predictions are $\Gamma^{2e/3}/\Gamma^{e/3} \approx \mathrm{e}^{-0.05(d/l_B)^2}$, $\Gamma^{2e/3}/\Gamma^{e/3} \approx \mathrm{e}^{-0.083(d/l_B)^2}$ respectively. Moreover, if we just plot the data for 10 electrons as in the inset of figure 4, it is shown that the deviation of the asymptotic behavior occurs near $L_x = 4.3l_B$ which is close to $\sim L_x^{c_2}$. This deviation also demonstrates that the tunneling has been affected by the edge–edge interaction at this length scale.

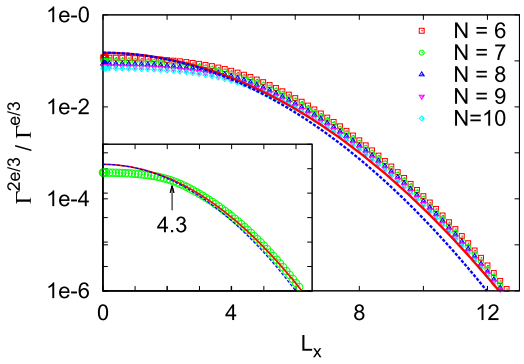

Figure 4. The ratio $\Gamma^{2e/3}/\Gamma^{2e/3}$ as a function of L_x. The dotted line is plotted using equation (5) and the solid line is the fitted line with $\Gamma^{2e/3}/\Gamma^{e/3} \approx e^{-0.078(x/l_B)^2}$. The inset is the enlarged part with smaller L_x for $N = 10$ electrons. The numerical data deviates from the asymptotic curve near $L_x^{c2} \simeq 4.3l_B$.

3. Bipartite entanglement entropy

The idea that the quantum entanglement [27] in a bipartite system can describe different phases of matter has emerged over the past few years. This approach has provided plenty of new insights, where traditional methods based on symmetry breaking and local order parameters in Landau theory have failed. More precisely, a bipartition of the quantum system is defined when the Hilbert space factors into two parts $\mathcal{H} = \mathcal{H}_A \otimes \mathcal{H}_B$. The bipartite FQH system can be implemented in both the momentum space and the real space of the two-dimensional electron system. The former is called the orbital cut (OC) [28] and the latter the real space cut (RC) [29]. With a bipartition, a pure quantum state $|\psi\rangle$ can be expressed in the form of the Schmidt decomposition

$$|\psi\rangle = \sum_i e^{-\xi_i/2} |\psi_i^A\rangle \otimes |\psi_i^B\rangle, \tag{6}$$

where $|\psi_i^A\rangle$ and $|\psi_i^B\rangle$ are orthonormal sets in $\mathcal{H}_A$ and $\mathcal{H}_B$ respectively and the value of ξ_i in the Schmidt singular values $e^{-\xi_i/2}$ are the entanglement 'energies' in the entanglement spectrum [30]. Equivalently, the reduced density matrix $\rho_A = \mathrm{tr}_B |\psi\rangle\langle\psi|$ has eigenvalues $\lambda_i = e^{-\xi_i}$. The Von Neumann entropy

$$S_A = -\mathrm{tr}\left[\rho_A \ln \rho_A\right] = -\sum_i \lambda_i \ln \lambda_i = \sum_i \xi_i e^{-\xi_i} \tag{7}$$

generally scales linearly with the area of the cut between parts A and B and with a universal order $O(1)$ correction, namely the topological entanglement entropy [31–33], i.e. $S = \alpha L - \gamma_t$. The topological entanglement entropy γ_t of the ground state for a fully gapped Hamiltonian is one robust measure of quantum entanglement in a topological phase in a two-dimensional system. In the FQH state, $\gamma_t = \log \mathcal{D}$ where $\mathcal{D} \geqslant 1$ is the total quantum dimension of the system. For the Laughlin state at $\nu = 1/3$, the quantum dimension is $\mathcal{D} = \sqrt{3}$ and therefore $\gamma_t \simeq 0.549306$.

On the cylinder, we intend to divide the system into two equal subsystems with the same number of orbitals in OC or the same length in RC. However, the number of orbitals for the N-electron Laughlin state is $N_{\mathrm{orb}} = 3N - 2$ which has the same parity as N. Then the bipartition of the orbitals should have an even–odd effect, which can be defined as the orbital difference between $\mathcal{H}_A$ and $\mathcal{H}_B$, namely $|N_{\mathrm{orb}}^A - N_{\mathrm{orb}}^B|$ is 0 for even N and is 1 for odd N. Intuitively, the effect of orbital difference should be diminished with increasing L_x due to the local properties of the entanglement entropy, or inversely, it becomes more clear in the small L_x or large L_y region. This can be seen in figure 5(c). In the RC case, it is easy to comprehend that an even–odd effect exists, especially in the thin cylinder limit. Taking the $N = 2$ and $N = 3$ thin cylinder crystal-like states as examples, their wavefunctions are single Slater-determinant $\Psi_{TT}(2) = |1001\rangle$ and $\Psi_{TT}(3) = |1001001\rangle$ respectively. Then the position of the RC cut for the state with even N has zero electron density which induces a zero entanglement entropy. On the other hand, there is an electron located at the position of the RC cut for the odd electron TT state. Then the electron density reaches its maximum and the entanglement entropy saturates at a specific value, which is the same as that for cutting a single electron wave function into two equal parts which is the classical Von Neumann entropy $S_{TT} = \log(2) \simeq 0.693147$ which is shown in figure 5(d). When the cylinder is bipartite along the y-direction, the L_y is actually the length of the cutting, or the 'area' between the two subsystems. Then the topological entanglement entropy γ_t can be extrapolated from figures 5(c) and (d). We found in the case of the OC that the data for the systems with the same parity are sitting on the same curve as a function of L_y. For large L_y, they can be fitted linearly and the topological entanglement entropies for even and odd parities are $\gamma_t \simeq 0.498$ and $\gamma_t \simeq 0.580$ respectively. The exact value $\gamma_t = \log \sqrt{3}$ is in between them. A more accurate

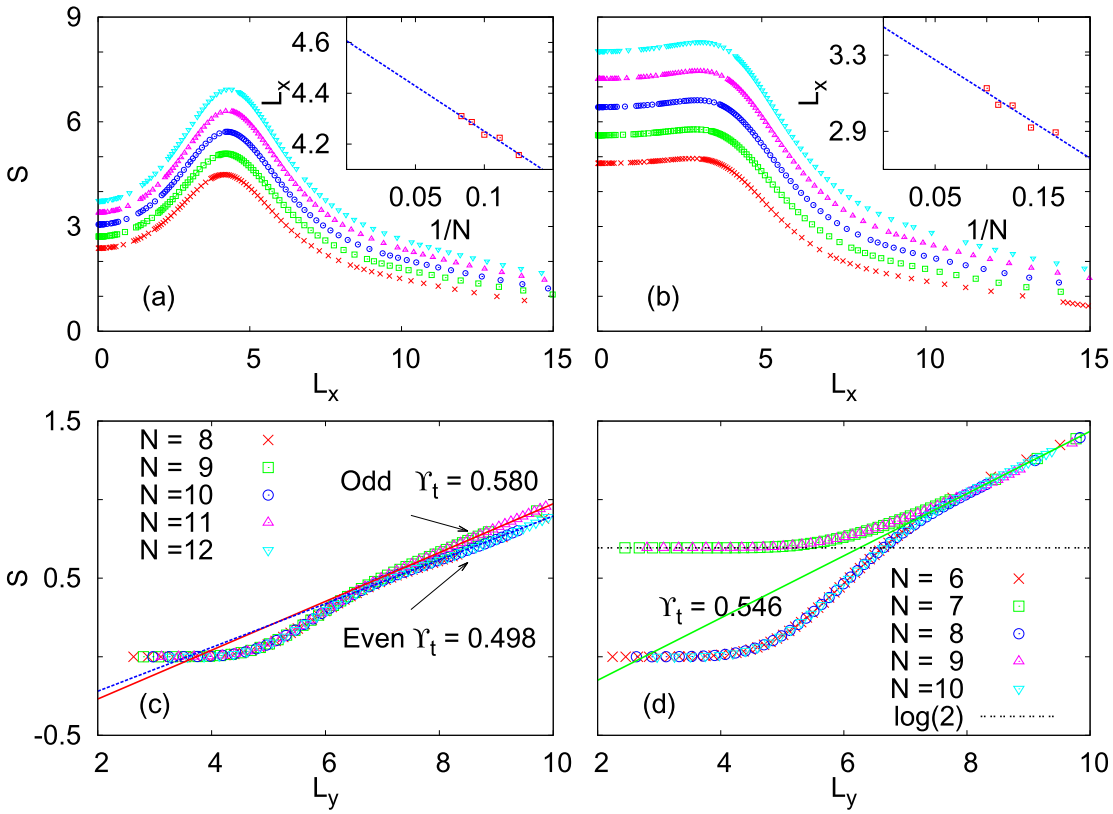

Figure 5. The entanglement entropy as a function of L_x in OC (a) and RC (b) and as a function of L_y in OC (c) and RC (d). The inset plot in (a) and (b) are the scaling of the position of the peak in the entropy. The plot in (c) has an even–odd effect in the large L_y region and the two fitting straight lines are $0.139L_y - 0.498 \pm 0.001$ (even) and $0.155L_y - 0.580 \pm 0.004$ (odd) respectively. The plot in (d) has an even–odd effect in small L_y region and the fitting line for large L_y is $0.198L_y - 0.546 \pm 0.006$.

extrapolation can be obtained in the RC entanglement entropy shown in figure 5(d) where $\gamma_t \simeq 0.546$, which is close to the exact value. An interesting phenomenon is that both the OC and RC entanglement entropies saturate at zero (log(2) for odd parity in RC) near $L_y \simeq L_x^{c_2}$. Therefore, we conclude that $L_x^{c_2}$ is the length scale in the y-direction where the CDW behavior appears.

In figures 5(a) and (b), we plot the bipartite entanglement with OC and RC as a function of L_x. The OC entanglement entropy has a peak at $L_x \simeq 4.6l_B$ in the thermodynamic limit as shown in the inset plot. In the RC, the peak of the entanglement entropy is not as sharp as that in the OC since the entropy while $L_x \to 0$ decreases very slowly. The position of the peak in the thermodynamic limit is $L_x \simeq 3.7 \pm 0.1l_B$. The error bar originates from the strong even–odd effect in this region. The difference between the OC and RC can be explained by the different width of the cuts in real space. The OC has a wider cut range and is more sensitive to the change of L_x. It is known that the entanglement entropy has a singularity at the critical point of the QPT due to the divergence of the quantum fluctuation. However, since no phase transition occurs while varying the L_x [21–23], the increment of the entanglement entropy originates from the correlations between the two edges. Therefore, the two length scales $L_x \simeq 4.6l_B$ and $L_x \simeq 3.7l_B$ for OC and RC respectively should be related to $L_x^{c_2} \simeq 4.2l_B$.

4. Electron Green's function

The tunneling characteristic at the edge has long been regarded as an experimental method by which to measure the topological order of the FQH liquids. For tunneling from a three-dimensional Fermi liquid into the FQH edge, chiral Luttinger liquid theory [34] leads to a non-Ohmic tunneling $I-V$ relation $I \propto V^{\alpha}$ with $\alpha \neq 1$, in sharp contrast to the Ohmic prediction of a Fermi-liquid-dominated edge with $\alpha = 1$. The electron Green's function is defined as

$$G(\mathbf{r} - \mathbf{r}') = \frac{\left\langle \psi \left| \Psi_e^{+}(\mathbf{r}) \Psi_e(\mathbf{r}') \right| \psi \right\rangle}{\langle \psi | \psi \rangle} \tag{8}$$

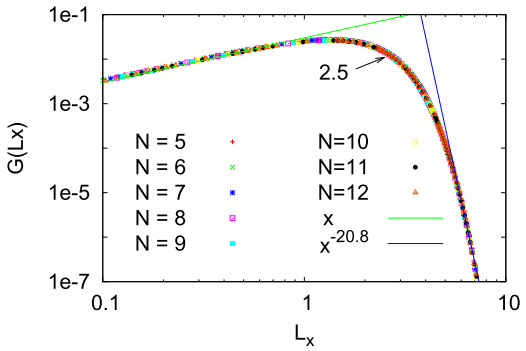

Figure 6. The log-log plot of the electron Green's function $|G(L_x)|$ for the Laughlin state for 5–12 electrons as a function of L_x. The data in the large and small L_x regions can be fitted by $\sim L_x^{-20.8}$ and $\sim L_x$ respectively. $L_x = 2.5l_B$ is the saddle point between these two phases.

where the $\Psi_e^+(\mathbf{r})$ and $\Psi_e(\mathbf{r}')$ are field operators which create and annihilate an electron at positions $\mathbf{r}$ and $\mathbf{r}'$ respectively. If we consider the tunneling path $|\mathbf{r} - \mathbf{r}'|$ along the edge of the FQH droplet, the edge Green's function shows a scaling behavior with $\alpha = 1/\nu$ for long distance tunneling [35, 36].

In this section, we consider the electron tunneling from the left edge of the cylinder to the right one, namely the electron correlation function between two anti-propagating edges as a function of L_x. The results are shown in figure 6. It shows that the Green's function decreases dramatically when L_x is larger than the saddle point which is the one-dimensional limit threshold value $L_x^{c_1} = 2.5l_B$. The data for the large tunneling distance near $L_x \sim 10l_B$ obeys a power law behavior with an exponent less than -20. In the large L_x limit, obviously, the Green's function is zero in the Tao–Thouless state which is an insulator. We also checked the $\nu = 1/5$ Laughlin state and found that the electron Green's function has the same power law behavior in this region. Thus we think that the exponent in the large L_x region depends on the interaction between electrons. The electron Green's function scales as a $G(L_x) \propto L_x$ which has a positive exponent of 1. Generally, the electron Green's function at zero temperature decays as $G(r) \sim r^{-1-\alpha}$ [37, 38] in which $\alpha \geqslant 0$ and $\alpha/2$ is the anomalous dimension of the fermion operators. The case for $\alpha = 0$ corresponds to the normal Fermi liquid and $\alpha > 0$ is due to the correction of the electron–electron interaction which is a characteristic behavior of a Luttinger liquid. On the other hand, when $L_x < L_x^{c_1}$, the system enters into a one-dimensional phase which is described by the Calogero–Sutherland model. The reason that the correlation decreases with reducing L_x is due to the repulsion between electrons, or strictly speaking, the electron Green's function drops to zero in the 1D limit.

5. Summary and discussion

In conclusion, we confirm that the quasihole tunneling amplitude in the cylinder geometry obeys the scaling conjecture in equation (4) and the scaling behavior is much better than that on a disk. Generally the scaling behavior works well when $L_x > L_x^{c_2}$ where $L_x^{c_2} \simeq 4.2l_B$ for $e/3$ and $L_x^{c_2} \simeq 5.2l_B$ for $2e/3$ with a difference due to the different size of the quasiholes. The $L_x^{c_2}$ can be explained as the threshold value of the edge–edge back scattering between the two edges. It appears not only in the quasihole tunneling amplitude calculations, but also in bipartite entanglement entropy. Therefore, the $L_x^{c_2}$ is the smallest length scale that guarantees there are two independent edges at the two ends of the cylinder. It should be the benchmark of the sample size in designing an experimental setup of the quasiparticle tunneling and interference [39, 40]. Moreover, we found another critical value $L_x^{c_1} \simeq 2.5l_B$, which is universal for different types of quasiholes. It can be explained as the critical width evolving from a 2D system to 1D system which is described by the Calogero–Sutherland model. Bipartite entanglement entropy has a singular behavior near $L_x^{c_2}$ due to a contribution of the edge–edge back scatterings. The topological entanglement entropy is extracted from the OC and RC entanglement entropies as a function of L_y in a finite-sized system. The $L_x^{c_1}$ plays the role of a saddle point in the single-particle Green's function where the system enters into a one-dimensional description. The scaling exponent of the Green's function is 1 while approaching the 1D limit. We notice that the $L_x^{c_1}$ is actually the correlation length of the Laughlin state as mentioned in the iDMRG calculation [41]. Here we should admit that we have only considered the Laughlin state of the model Hamiltonian with hardcore interaction, or with V_1 pseudopotential. For a realistic coulomb interaction or the FQH state in higher Landau levels, we believe that similar behaviors exists which may at most have small modifications on the value of these length scales.

Acknowledgments

We thank X Wan and G T Liu for helpful discussions. This work was supported by NSFC Project No. 1127403 and Fundamental Research Funds for the Central Universities No. CQDXWL-2014-Z006. NJ is also supported by Chongqing Graduate Student Research Innovation Project No. CYB14033.

References

[1] Tsui D C, Stomer H L and Gossard A C 1982 *Phys. Rev. Lett.* **48** 1559
[2] Kitaev A 2003 *Ann. Phys.* **303** 2
[3] Freedom M H 1998 *Proc. Natl Acad. Sci. USA* **95** 98
[4] Nayak C, Simon S H, Stern A, Freedom M and Das Sarma S 2008 *Rev. Mod. Phys.* **80** 1803
[5] de C Chamon C, Freed D E, Kivelson S A, Sondhi S L and Wen X G 1997 *Phys. Rev.* B **55** 2331
[6] Stern A and Halperin B I 2006 *Phys. Rev. Lett.* **96** 016802
[7] Bonderson P, Kitaev A and Shtengel K 2006 *Phys. Rev. Lett.* **96** 016803
[8] Chen H, Hu Z-X, Yang K, Rezayi E H and Wan X 2009 *Phys. Rev.* B **80** 235305
[9] Hu Z-X, Lee K-H, Rezayi E H, Wan X and Yang K 2011 *New J. Phys.* **13** 035020
[10] Hu Z-X, Lee K-H and Wan X 2012 *Int. J. Mod. Phys. Conf. Ser.* **11** 70
[11] Tao R and Thouless D J 1983 *Phys. Rev.* B **28** 1142
[12] Thouless D J 1984 *Surf. Sci.* **142** 147
[13] Rezayi E H and Haldane F D M 1994 *Phys. Rev.* B **50** 17199
[14] Feigin B, Jimbo M, Miwa T and Mukhin E 2002 *Int. Math. Res. Not.* **2002** 1223
Feigin B, Jimbo M, Miwa T and Mukhin E 2003 *Int. Math. Res. Not.* **2003** 1015
[15] Bernevig B A and Haldane F D M 2008 *Phys. Rev. Lett.* **100** 246802
[16] Bernevig B A and Haldane F D M 2008 *Phys. Rev. Lett.* **101** 246806
[17] Bernevig B A and Regnault N 2009 *Phys. Rev. Lett.* **103** 206801
[18] Lee K-H, Hu Z-X and Wan X 2014 *Phys. Rev.* B **89** 165124
[19] Yang B, Hu Z-X, Papić Z and Haldane F D M 2012 *Phys. Rev. Lett.* **108** 256807
[20] Hu Z-X, Papic Z, Johri S, Bhatt R N and Schmitteckert P 2012 *Phys. Lett.* A **376** 2157
[21] Seidel A, Fu H, Lee D-H, Leinaas J M and Moore J 2005 *Phys. Rev. Lett.* **95** 266405
[22] Bergholtz E J and Karlhede A 2008 *Phys. Rev.* B **77** 155308
[23] Bergholtz E J, Hansson T H, Hermanns M, Karlhede A and Viefers S 2008 *Phys. Rev.* B **77** 165325
[24] Calogero F 1969 *J. Math. Phys.* **10** 2197
Sutherland B 1971 *J. Math. Phys.* **12** 246
Sutherland B 1971 *J. Math. Phys.* **12** 251
[25] Jain J K 1990 *Phys. Rev.* B **41** 7653
[26] Yu Y 2000 *Phys. Rev.* B **61** 4465
[27] Nielsen M A and Chuang I L 2000 *Quantum Computation and Quantum Information* (Cambridge: Cambridge University Press)
[28] Haque M, Zozulya O and Schoutens K 2007 *Phys. Rev. Lett.* **98** 060401
Zozulya O S *et al* 2007 *Phys. Rev.* B **76** 125310
[29] Dubail J, Read N and Rezayi E H 2012 *Phys. Rev.* B **85** 115321
Sterdyniak A, Chandran A, Regnault N, Bernevig B A and Bonderson P 2012 *Phys. Rev.* B **85** 125308
[30] Li H and Haldane F D M 2008 *Phys. Rev. Lett.* **101** 010504
[31] Hamma A, Ionicioiu R and Zanardi P 2005 *Phys. Lett.* A **337** 22
[32] Kitaev A and Preskill J 2006 *Phys. Rev. Lett.* **96** 110404
[33] Levin M and Wen X G 2006 *Phys. Rev. Lett.* **96** 110405
[34] Wen X G 1992 *Int. J. Mod. Phys.* B **6** 1711
[35] Wan X, Evers F and Rezayi E H 2005 *Phys. Rev. Lett.* **94** 166804
[36] Hu Z-X, Bhatt R N, Wan X and Yang K 2012 *J. Phys.: Conf. Ser.* **402** 012017
[37] Luther A and Peschel I 1974 *Phys. Rev.* B **9** 2911
[38] Theumann A 1967 *J. Math. Phys.* **8** 2460
[39] Willett R L, Pfeiffer L N and West K W 2009 *Proc. Natl Acad. Sci. USA* **106** 8853
[40] Willett R L, Pfeiffer L N and West K W 2010 *Phys. Rev.* B **82** 205301
[41] Zaletel M P, Mong R S K, Pollman F and Rezayi E H 2015 *Phys. Rev.* B **91** 045115